JOURNAL OF CATALYSIS **158,** 363–377 (1996)
ARTICLE NO. 0038

Interaction of Oxygen with Supported Ag–Au Alloy Catalysts

Dimitris I. Kondarides and Xenophon E. Verykios

Department of Chemical Engineering and Institute of Chemical Engineering and High Temperature Chemical Processes, University of Patras, P.O. Box 1414, GR-26500 Patras, Greece

Received December 6, 1994; revised September 1, 1995; accepted September 26, 1995

The effects of alloying silver with gold on the oxygen adsorption properties of Ag are studied over a set of 15% (Ag–Au)/α-Al_2O_3 catalysts of variable alloy composition, using microgravimetric and temperature desorption techniques. Three adsorbed oxygen species are observed on the alloy surfaces at elevated temperatures, namely molecular, atomic and subsurface. It is found that geometric and electronic alterations induced by the presence of Au influence the adsorption characteristics differently for each species. When the Au content of the surface increases, the population of atomic oxygen decreases, its activation energy of adsorption increases, and the Ag–O bond weakens, while the enthalpy of adsorption decreases linearly from approximately 170 kJ/mol over pure Ag to about 70 kJ/mol over surfaces containing 24 at.% Au. Molecular oxygen adsorption on Ag is favored by the presence of Au, as indicated by the decrease of its activation energy of adsorption with increasing Au content. Finally, subsurface oxygen diffusion is strongly inhibited by the presence of gold, and the activation energy of this process increases from 100 kJ/mol for pure Ag to 400 kJ/mol for samples containing 24 surface at.% Au. These results are discussed evoking geometric and electronic alterations induced by the presence of Au on the catalytic surfaces.

INTRODUCTION

The unique ability of silver to selectively catalyze the partial oxidation of ethylene to ethylene oxide has attracted scientific interest in this system for several decades. Although ethylene epoxidation over silver surfaces has been extensively studied and selectivity has exceeded 80% in industrial processes, research is still continued in the field mainly for two reasons: First, there is no thermodynamic limit for further increasing selectivity to ethylene oxide and, second, many fundamental questions concerning the mechanism of the reaction still remain unanswered. As a result, the various mechanistic steps involved in the process, such as oxygen adsorption on Ag, reaction of the adsorbed oxygen species with ethylene, and formation and reaction of surface intermediates, are still subjects of investigation (1–5). The key role of oxygen adsorption on silver has been realized since the early studies, and several publications deal with the number and nature of adsorbed oxygen species, under reaction conditions, and their role in the epoxidation and combustion routes. The role of well-known promoters used in the industrial processes to improve selectivity to ethylene oxide, such as chlorine and alkali and alkaline earth metals, has been related to alterations of the chemisorptive properties of silver due to electronic and geometric modifications induced by the additives on the catalytic surface (1–5). Another approach to studying and understanding the nature and the role of the adsorbed oxygen species and to gaining information concerning the mechanism of the ethylene epoxidation reaction is modifying the properties of the catalytic surfaces by alloying. Upon alloying, special adsorption sites may be created or destroyed and electronic interactions may be induced due to the electronegativity differences of the alloy components. Among the metals employed by researchers in similar studies are Au, Pd, Cd, and Zn (6–11).

In our previous work (12–14) we have employed surface-enhanced Raman spectroscopy, microgravimetric, and transient techniques with the use of isotopically labeled oxygen to study oxygen adsorption on Ag/α-Al_2O_3 catalysts at atmospheric pressure and elevated temperatures. It was shown that three oxygen species exist in the adsorbed mode under reaction conditions, viz., molecular, atomic, and subsurface.

In the present work we extend our study of the silver–oxygen system by examining the effect of alloying silver with gold on the adsorption characteristics of silver using microgravimetric and temperature desorption techniques. Gold was chosen due to its ability to form solid solutions with silver at any composition and because of its inertness toward oxygen adsorption and ethylene oxidation. The results of the present study confirm the presence of three adsorbed oxygen species at elevated temperatures and show that alloying Ag with Au influences bond strengths with the silver surface and, thus, modifies the relative population of the adsorbed species.

0021-9517/96 $12.00

EXPERIMENTAL

(*i*) *Catalyst Preparation*

Supported Ag catalysts were prepared by impregnation of low-surface-area (~1 m^2/g) α-Al_2O_3 (Alfa Products) with Cl-free $AgNO_3$ (Alfa products), following a procedure which has been described elsewhere (13). Supported silver–gold alloy catalysts were prepared by simultaneous impregnation of the support with AgCN and AuCN (Alfa Products). Silver and gold cyanides were used in order to avoid contamination of the alloy catalysts with chlorine, which is known to be a promoter of the epoxidation reaction. Known amounts of the salts, calculated to give the desired Ag–Au composition to the final product, were dissolved in an aqueous solution of ethylenediamine (Ferak). The carrier was then added under continuous stirring, and the resulting mixture was slowly heated to 70°C and maintained at that temperature until nearly all of the liquid had evaporated. The slurry was dried overnight at 110°C and subsequently calcined in air, at 400°C, for 8 h. After this treatment the solids were ground and sieved in the particle size range between 65 and 125 μm. The total metal loading of all samples was 15 wt% with gold content 0, 10, 30, 50, 70, and 100 (wt%), based on total metal loading. For simplicity, in the following paragraphs the silver–gold alloy catalysts will be referred to using the percentage weight of the metals in parentheses, e.g., Ag–Au (70–30).

(*ii*) *Catalyst Characterization Techniques*

The extent of alloying of Ag–Au catalysts was examined using X-ray diffraction (XRD). Spectra were obtained with a Philips PW 1830/40 diffractometer equipped with a Cu radiation source [$\lambda(K_{\alpha_1})$ = 1.542 Å] and a Ni filter. The samples, in powder form, were placed in an aluminum pan, and spectra were obtained in the angle range between 30 and 80° (2θ), with a scanning rate of 0.01° s^{-1}. In this angular range, the characteristic diffraction peaks due to the (111), (200), (220), and (311) lattice planes of the alloys were observed at diffraction angles (2θ) of approximately 38.0, 44.0, 64.5, and 77.5°, respectively. The accuracy of the instrument is 0.02°(2θ).

The crystallite size and surface morphology of all samples were examined employing a Jeol (JSM-5200) scanning electron microscope. A small portion of each sample powder was coated on a metallic disk holder and covered with a thin gold layer. Several SEM pictures of the catalyst surfaces were obtained for each sample.

Surface composition of the Ag–Au alloy crystallites was studied with XPS using the AlK_α line (1468 eV) of a Mg/Al double-anode X-ray source. With this technique, the samples containing 10, 30, 50, and 70 wt% Au were examined. In all cases, the characteristic O 1*s* and Al 2*p* peaks of the carrier and the Ag $3d_{3/2}/3d_{5/2}$ and Au $4f_{5/2}/4f_{7/2}$ of the metals were observed. Carbon C $1s_{1/2}$ (284.6 eV) was used to calibrate binding energies. The Ag/Au ratio was calculated from the relative intensities of the Ag $3d_{5/2}$ and Au $4f_{7/2}$ photoelectron peaks using the equation

$$N_{Au}/N_{Ag} = (I^{\infty}_{Ag}/I^{\infty}_{Au})(I_{Au}/I_{Ag}) = 1.07(I_{Au}/I_{Ag}), \quad [1]$$

where $N_{Ag,Au}$ is the number of atoms of each component in the sample contributing to the XPS signal, $I_{Ag,Au}$ is the measured intensity of the photoelectron peaks, and $I^{\infty}_{Ag,Au}$ is the relative intensity of the peaks of the pure metals which was calculated from data tables (15) and depends on the mean free path of the photoelectrons in the metal, the scattering cross section of the emission process, the kinetic energy of the photoelectrons, and a correction factor for the presence of surface carbon.

(*iii*) *Gravimetric Experiments*

A Cahn C-2000 vacuum ultramicrobalance was employed to study the kinetics of oxygen adsorption on the 15% (Ag–Au)/α-Al_2O_3 catalysts in the temperature range of 40 to 320°C, at a constant oxygen pressure of 50 Torr. The apparatus and procedure have been described in detail elsewhere (13). In a typical experiment the sample was placed in an aluminum pan and exposed to a number of oxidation–evacuation–reduction–evacuation cycles which have been found to be necessary for cleaning and stabilizing the catalytic surface and for obtaining reproducible results (13). The sample was then heated to 320°C, reduced *in situ* at the same temperature under 300 Torr hydrogen for 8 h, and cooled to the desired adsorption temperature. After the balance chamber was evacuated for 3 h, 50 Torr of oxygen was introduced to the system and the weight increase of the catalyst due to oxygen adsorption was continuously recorded for 15 h through a personal computer interfaced to the weighing unit. Blank experiments using 50 Torr of N_2 instead of O_2 were performed in all cases in order to correct the raw data from the buoyancy and ''initial shock'' effects occurring when the gas was introduced to the evacuated chamber (13). Preliminary experiments showed no measurable mass uptake of oxygen on the α-Al_2O_3 carrier or on the Ag–Au (0–100) sample. Each experiment was conducted at least two times, and all results reported were reproducible. The accuracy of the measurements is $\pm$0.1 μg.

(*iv*) *Temperature-Programmed Desorption* (*TPD*)

The TPD experiments were conducted following oxygen adsorption at temperatures between 25 and 400°C in an apparatus which has been described elsewhere (13). Pretreatment of the catalysts was identical to that used in the gravimetric experiments. In a typical TPD experiment,

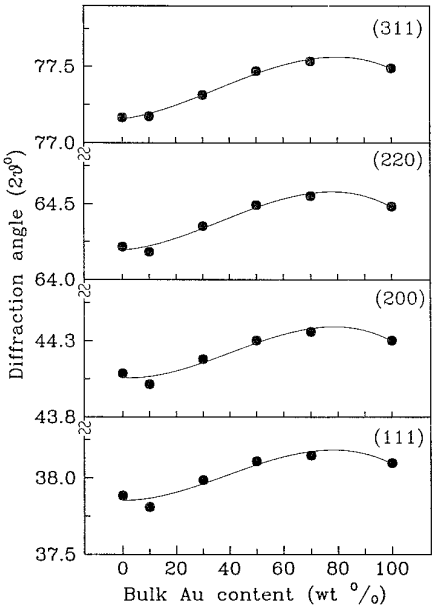

FIG. 1. Dependence of the X-ray diffraction angle, 2θ, of the (111), (200), (220), and (311) crystallographic planes, on the Au content of Ag–Au/α-Al_2O_3 alloy catalysts.

after pretreatment, the sample was heated to the desired adsorption temperature under He flow and exposed to oxygen flow for 30 min. The catalyst was then cooled to room temperature under oxygen flow, and the tubing was flushed with He, bypassing the reactor, until no oxygen was detected at the effluent. Helium flow was then permitted through the reactor via a six-way valve for 5 min, the time required to remove the gas phase oxygen, as was determined in preliminary experiments. Temperature-programmed desorption of adsorbed oxygen was then followed by heating the sample from room temperature to 650°C with a constant heating rate between 20 and 100°C/min under a He flow of 40 ml/min. The effluent of the reactor was connected to a VG Sensorlab-2000 quadrupole mass spectrometer interfaced to a personal computer. Desorbed oxygen was monitored at $m/z = 32$, while no other gases were observed to desorb from the catalyst surfaces during the TPD experiments. All gases used (O_2, H_2, N_2, He) were of ultra high purity, provided by L'Air Liquide, and were further purified with the use of appropriate traps.

RESULTS

(*i*) *Catalyst Characterization*

(*a*) *Bulk composition.* The degree of alloying of the Ag–Au crystallites was examined with XRD. For all samples examined, only one of the characteristic diffraction peaks due to the (111), (200), (220), and (311) lattice planes of Ag and Au was observed. The absence of a second XRD peak for each diffraction plane (one for Ag and one for Au) indicates that complete alloying had occurred following the preparation procedure which was described earlier. This is expected, since both Ag and Au crystallize in the fcc form and have comparable atomic size and electronegativity, thus forming solid solutions over the entire composition range. The dependence of the diffraction angle, 2θ, due to the four lattice planes examined, on the composition of the Ag–Au crystallites is illustrated in Fig. 1. It is observed that for all diffraction planes, the presence of Au induces a shift of the diffraction peaks toward higher diffraction angles, which continues up to alloy compositions of about 70 wt% Au. A shift of the diffraction peaks in the opposite direction occurs at higher Au content. The accuracy of the measurements is $\pm 0.02°$ (2θ), and the error bars of the data points of Fig. 1 are equal to the diameter of the symbols used, indicating that the decrease in angle at high Au levels is real. The lattice constant, a_0, for each sample was calculated for all four diffraction planes. A more accurate value was obtained by plotting the calculated a_0 values versus $\sin^2\theta$ and extrapolating to $\sin^2\theta = 0$ (16). The lattice constants of the Ag–Au crystallites calculated in this manner are shown as a function of Au composition in Fig. 2. The values of the lattice constant are in agreement with those of bulk Ag–Au alloys of similar composition reported in the literature (17). Small differences can be attributed to the fact that in the present study, relatively small alloy particles are employed as opposed to massive alloys. As observed in Fig. 2, the curve passes through a minimum for catalysts with approximately 70 wt% Au, in accordance with results of other studies [6–8].

(*b*) *Surface composition.* It is well known that the surface composition of alloy particles can vary significantly from that of the bulk. In most cases, the surface of an alloy is enriched with one of its components. The driving force for this process is the minimization of the total free energy of the system (18). Thus, the surface of the alloy is enriched

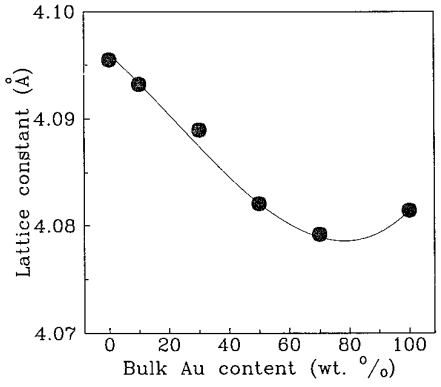

FIG. 2. The effect of Ag–Au composition on the lattice parameter, a_0, of alloy crystallites.

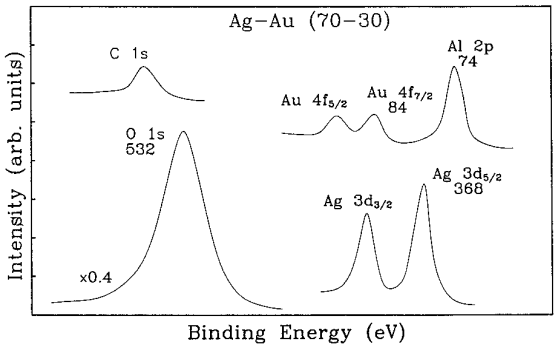

FIG. 3. Typical X-ray photoelectron spectra obtained from the Ag–Au (70–30) catalyst.

with the component with the lower surface free energy. Another parameter that may affect the surface composition is selective chemisorption of a gas on the components of the alloy. The component that interacts more strongly with the ambient gas could diffuse and enrich the surface. In the case of the Ag–Au alloy catalysts both parameters lead to enrichment of the surface with Ag. Silver has a lower surface free energy (1140 erg/cm^2 at 907°C) than gold (1410 erg/cm^2 at 1027°C) (18), so, during preparation, the alloy catalysts were calcined in air at 400°C for 8 h. Oxygen is strongly adsorbed on Ag but not on Au, thus favoring the enrichment of the alloy crystallite surfaces with the former component.

A typical XPS spectrum obtained from the Ag–Au (70–30) catalyst is presented in Fig. 3, in which the characteristic peaks of the sample components are shown. The results of all XPS experiments which were carried out are presented in Fig. 4. The dependence of the experimentally measured XPS intensity ratio, I_{Au}/I_{Ag}, of the Au $4f_{7/2}$ and Ag $3d_{5/2}$ peaks, on the ratio of the atoms of the metals in the bulk is shown in Fig. 4(I, b). For comparison purposes, the expected intensity ratio of the same peaks for two extreme cases is also presented: (i) the surface composition of the sample is the same as that of the bulk [Fig. 4(I, a)], and (ii) the composition of the surface is the same as that of the bulk but covered with a thin Ag layer with a thickness of 5 Å [Fig. 4(I, c)]. The difference between curves (a) and (b) of Fig. 4(I) indicates that the surface of the Ag–Au alloy crystallites is indeed enriched with Ag, for the reasons discussed above. The uppermost surface layer, which is the most important from the catalytic point of view, is probably more enriched in Ag than indicated by curve [4(I, b)] because the XPS technique does not have the surface sensitivity of other techniques like ISS, which is sensitive to the first surface layer only. The information obtained by the XPS experiments covers a depth of about 3λ. In the case of Ag ($\lambda_{Ag3d_{5/2}}$ = 11.7 Å) this depth corresponds to about 10 atomic silver layers (19). In the endothermically formed alloys, surface enrichment is mainly limited to the first one or two surface layers (19), but since the process of alloying Ag with Au is slightly exothermic this seems not to be the case here. Comparison of curves (a–c) of Fig. 4(I) shows that there is surface enrichment with Ag, but this enrichment is not restricted to the topmost layers. Theoretical calculations for predicting the surface composition cannot be applied in this case since the models that have been proposed to simulate the enrichment of the surface of the alloys in one component cannot be applied to supported bimetallic catalysts because of the influence of many parameters like the preparation method, temperature, crystallite size, and the nature of the carrier (20).

Assuming that the detected XPS signal originates from surface layers with the same Ag–Au composition, the values shown in Fig. 4(II, b) are obtained. It has to be kept in mind that this assumption is only made to obtain a direct estimate of surface composition from bulk alloy composition. Since the XPS signal decreases exponentially with the distance of the examined atoms from the surface, it is expected that the values obtained mainly refer to the composition of the topmost surface layers of the alloy. As discussed before, the exothermic nature of the formation of Ag–Au alloys indicates that although segregation of Ag in the top layers occurs, it is not expected to be extreme,

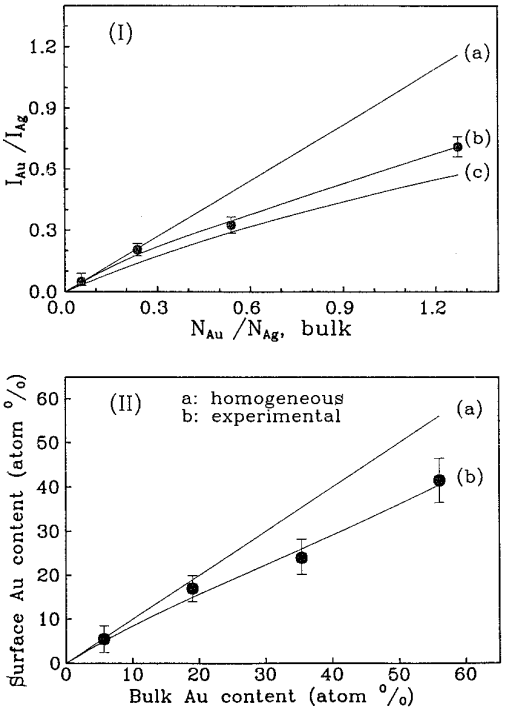

FIG. 4. (I) The dependence of the relative intensity, I_{Au}/I_{Ag}, of the Au $4f_{7/2}$ and Ag $3d_{5/2}$ photoelectron peaks on the Ag–Au alloy composition. (a) Homogeneous alloy; (b) experimental results; (c) homogeneous Ag–Au alloy covered by a 5 Å thick surface Ag layer. (II) Surface versus bulk Au content of the Ag–Au alloy crystallites. (a) homogeneous; (b) experimental.

TABLE 1

Characterization of the 15% (Ag–Au)/α-Al_2O_3 Catalysts

wt% Au (bulk)	at.% Au (bulk)[a]	at.% Au (surface)[b]	Crystallite size (nm)[c]	Ads O_2 at $\theta = 1$ (μg/g cat.)[d]	Exposed Ag area (m^2/g cat.)	Surf. Ag atoms ($\times 10^{18}$ atom/g cat.)
0	0	0	97	141.0	0.462	5.31
10	5.5	5	84	75.7	0.239	2.75
30	19.0	15	99	56.0	0.183	2.11
50	35.5	24	94	42.2	0.138	1.59
70	56.0	40	98	19.8	0.065	0.75
100	100	100	91	—	—	—

[a] Calculated from the wt% Au composition.
[b] Calculated from the XPS measurements (Fig. 4).
[c] Obtained from XRD measurements.
[d] Equilibrium oxygen adsorption at 200°C.

as in the case of endothermically formed alloys. Thus, the actual surface composition of the alloys is not expected to be much different from that shown in Fig. 4(II). The surface composition of the samples obtained under this assumption [Fig. 4(II), Table 1] will be used in the following paragraphs.

(*c*) *Crystallite size.* The mean crystallite size of the Ag–Au catalysts was calculated from the XRD data using the Scherrer equation (16) and the results are presented in Table 1. It is observed that the average size of the Ag–Au alloy crystallites is almost independent of alloy composition and is in the neighborhood of 100 nm. This finding was also confirmed by SEM experiments. The relatively large size of the Ag–Au crystallites is due to the low surface area of α-Al_2O_3 and the large metal loading of the catalysts. The similar mean diameter of the alloy crystallites (Table 1) and the lack of a trend correlating the crystallite size with alloy composition indicate that, although the total metal atom content is different (due to the differences in atomic weights of Ag and Au), the alloy composition does not influence measurably the crystallite morphology. In fact, it has been found that the dependence of Ag surface area on loading for Ag/α-Al_2O_3 catalysts is nonlinear, especially for high metal loadings, which is attributed to the absence of strong interactions of the metal precursor with the support (21). Since this condition also holds for the Ag–Au/α-Al_2O_3 catalysts, it is reasonable to expect the formation of crystallites with approximately the same size, in spite of small differences in the total atom metal content.

(*d*) *Exposed Ag surface area.* The exposed silver surface area of the 15% (Ag–Au)/α-Al_2O_3 catalysts was determined with selective oxygen chemisorption measurements using the gravimetric technique. Oxygen adsorption measurements were obtained in the temperature range of 40 to 320°C under an oxygen pressure of 50 Torr. The dependence of the equilibrium oxygen uptake on adsorption temperature for all Ag–Au alloy catalysts is shown in Fig. 5. Equilibrium uptake was obtained following the procedure described in a previous paragraph, 15 h after the introduction of 50 Torr O_2 to the reduced samples, when adsorption had reached equilibrium. Since no measurable mass uptake was observed to occur on unmetallized α-Al_2O_3 and the Ag–Au (0–100) sample, the mass uptake was attributed to oxygen adsorption on Ag. As observed in Fig. 5 (curves a–e), the amount of oxygen adsorbed decreases with increasing Au content at all adsorption temperatures. In all cases the adsorption curves pass through a maximum at adsorption temperatures of about 200–220°C, while there is a new increase in the amount of oxygen uptake at temperatures above 250°C for the Ag–Au (100–0) and (90–10) samples [Fig. 5 (curves a, b)]. In a previous study (13) we have attributed this high-temperature oxygen uptake to the initiation of a new process, namely oxygen diffusion to subsurface sites, which becomes significant at elevated temperatures. Gavriilidis *et*

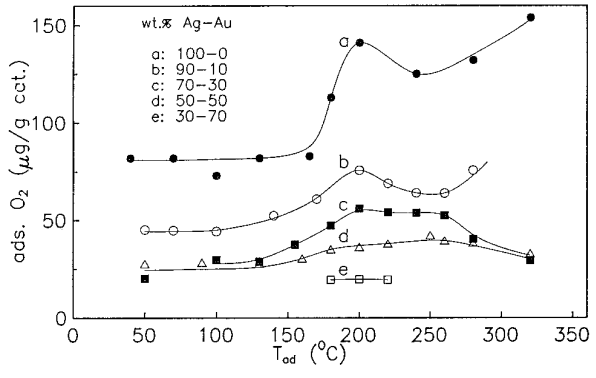

FIG. 5. Equilibrium uptake of oxygen adsorbed on the 15% (Ag–Au)/α-Al_2O_3 catalysts as a function of adsorption temperature. $P_{O_2} = 50$ Torr.

al. (21) performed oxygen adsorption experiments in the temperature range of 120 to 240°C on a 14% Ag/α-Al_2O_3 catalyst and observed a similar equilibrium adsorption curve with a maximum at 200°C. The authors do not report data at adsorption temperatures above 240°C where a second increase in oxygen uptake is initiated, as shown in Fig. 5.

The maximum oxygen uptake, at 200°C, is usually used to calculate the exposed surface area of Ag catalysts, assuming monolayer coverage and a 1:1 adsorption stoichiometry (22, 23). An inaccuracy arises from the fact that oxygen can be present in the adsorbed mode as atomic, molecular, and/or subsurface, occupying mono and/or multicoordinated sites (1–5). Unfortunately, the most commonly used gases for selective chemisorption measurements, like H_2 and CO, do not give a monolayer coverage when adsorbed on Ag surfaces at elevated temperatures and cannot be used for this purpose. As will be shown in a following paragraph, TPD experiments show that the amount of the subsurface oxygen on the Ag–Au (100–0) sample at 200°C is small compared to the total amount of adsorbed oxygen and negligible for the gold-containing samples.

Based on these observations and in accordance with previous studies, it is assumed that the maximum oxygen uptake observed at 200°C in the adsorption curves of Fig. 5 corresponds to monolayer coverage of oxygen adsorbed on the alloy surfaces. The calculated quantity of adsorbed oxygen at monolayer coverage for the 15% (Ag–Au)/α-Al_2O_3 catalysts is shown in Table 1. The corresponding Ag surface atoms per gram of catalyst, assuming a 1:1 ratio between Ag and O atoms, and the exposed Ag surface area of the alloys, calculated based on the number of Ag atoms per unit area (1.15×10^{19} m^{-2}) for polycrystalline Ag films (24), are also shown in Table 1.

(*ii*) *Gravimetric Experiments*

The oxygen adsorption curves obtained from the Ag–Au (100–0), (90–10), (70–30), and (50–50) catalysts in the temperature range of 40 to 320°C are shown in Fig. 6, graphs I–IV, respectively. It is observed that in all cases there is an initial rapid mass uptake due to fast oxygen adsorption followed by a gradually decreasing adsorption rate which continues for several hours before reaching a plateau after approximately 15 h. The initial rapid mass uptake becomes more pronounced with increasing adsorption temperature and decreases with increasing Au content. As was shown in a previous study (13), the adsorption curves can be analyzed using the Elovich equation. The applicability of the Elovich equation is usually tested using the integrated form

$$\theta = 1/\gamma \cdot \ln(t + t_0) - 1/\gamma \cdot \ln t_0, \qquad (2)$$

where $t_0 = (\beta\gamma P)^{-1}$, θ is the surface coverage at any time t, β and γ are temperature-dependent parameters, and P is the oxygen pressure. For large values of t (i.e. $t \gg t_0$), the plot of θ against ln t is linear, and values of β and γ may be derived from the slope and the intercept (25). In the present experiments, t_0 is typically much lower than 2 min, and the integrated Elovich equation can be applied to determine the values of these parameters. The data of Fig. 6 plotted in the coordinates of the integrated Elovich equation are shown in Fig. 7. In all cases the curves consist of two intersecting linear segments, indicating the existence of at least two kinetically distinguishable adsorption processes (13). From the slope and intercept of the linear segments of Fig. 7, the temperature-dependent parameters β and γ were estimated for all catalysts employed in the present study.

The values of β which were thus obtained for the Ag–Au (100–0), (90–10), (70–30), and (50–50) catalysts are shown in Arrhenius-type diagrams in Fig. 8. Lines designated as (a) were obtained from the first (low time values) linear segments of Fig. 7 while the lines designated as (b) were obtained from the second (high time values) segments. It is observed that for all catalysts the calculated β values of the (b) segments shown in Fig. 8 lie on a straight line. These data have previously been attributed to a molecular oxygen adsorption process (13), while the data from the (a) segments which can be fitted by two intersecting straight lines were argued to be due to an atomic oxygen adsorption and a subsurface oxygen diffusion process, respectively (13). The point of intersection of the (a) data points shifts toward higher temperatures with increasing Au content, from approximately 165°C for the Ag–Au (100–0) sample [Fig. 8(I)] to approximately 260°C for the Ag–Au (50–50) sample [Fig. 8(IV)].

The activation energy of adsorption of the oxygen species at zero surface coverage can be calculated from the slope of the linear segments of Fig. 8 (13). The calculated values for the activation energy of adsorption of the three kinetically distinguishable oxygen adsorption processes are shown in Fig. 9. It is observed that increasing Au content from 0 to 50 wt% results in an increase of the activation energy (at zero surface coverage) of atomic oxygen from 4 to 40 kJ/mol, a decrease of the corresponding value for molecular oxygen from 44 to 17 kJ/mol, and an increase of the activation energy of subsurface oxygen diffusion from 100 to almost 400 kJ/mol.

(*iii*) *Temperature-Programmed Desorption Studies*

Temperature-programmed desorption experiments for all Ag–Au/α-Al_2O_3 catalysts were conducted following oxygen adsorption in the temperature range of 25 to 400°C using the apparatus and procedure described in a previous section. The TPD profiles ('spectra'), which were obtained

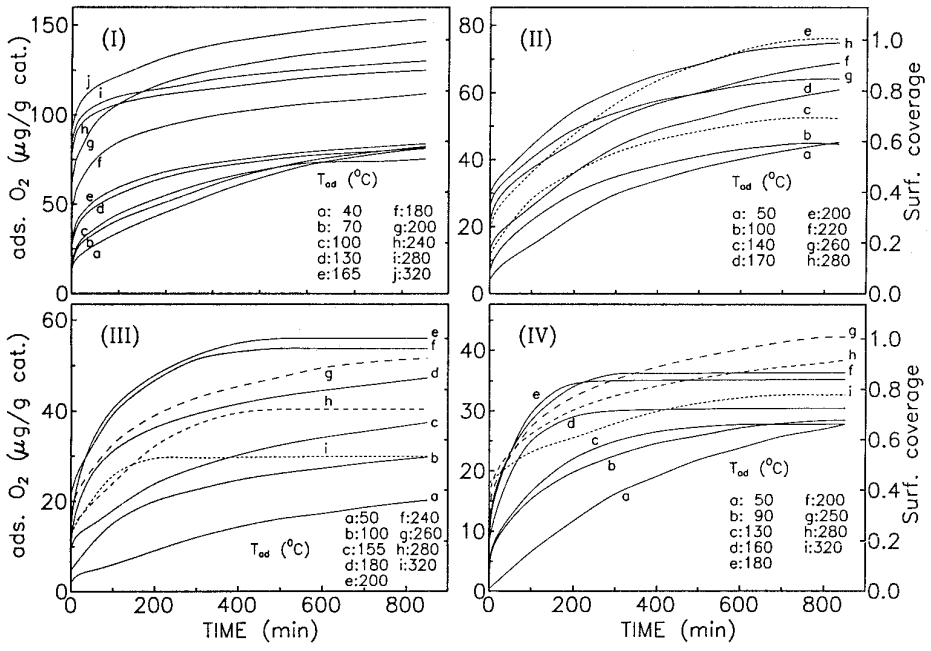

FIG. 6. Oxygen adsorption curves on prereduced 15% (Ag–Au)/α-Al_2O_3 surfaces in the temperature range of 40 to 320°C. Ag–Au composition (wt%): (I) 100–0; (II) 90–10; (III) 70–30; (IV) 50–50; P_{O_2} = 50 Torr.

with a heating rate of 20°C/min, are shown in Fig. 10(I–IV). Three different TPD features can be observed depending on the adsorption temperature and the Ag–Au alloy composition. In all cases a weakly adsorbed oxygen species is observed to desorb at temperatures below 150°C. Rehren *et al.* (26) have also observed a TPD feature at 150°C in their desorption experiments from a Ag film after oxygen adsorption at room temperature which, after blank experiments, was attributed to oxygen adsorption on the metallic walls of their apparatus. In the present case, it was con-

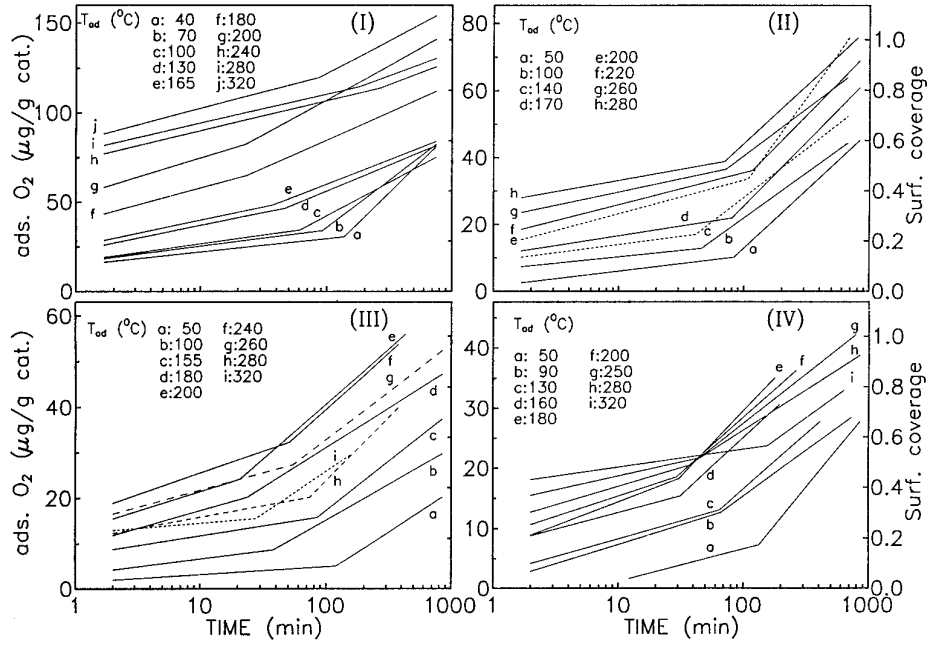

FIG. 7. The adsorption curves of Fig. 6 plotted in the coordinates of the integrated Elovich equation.

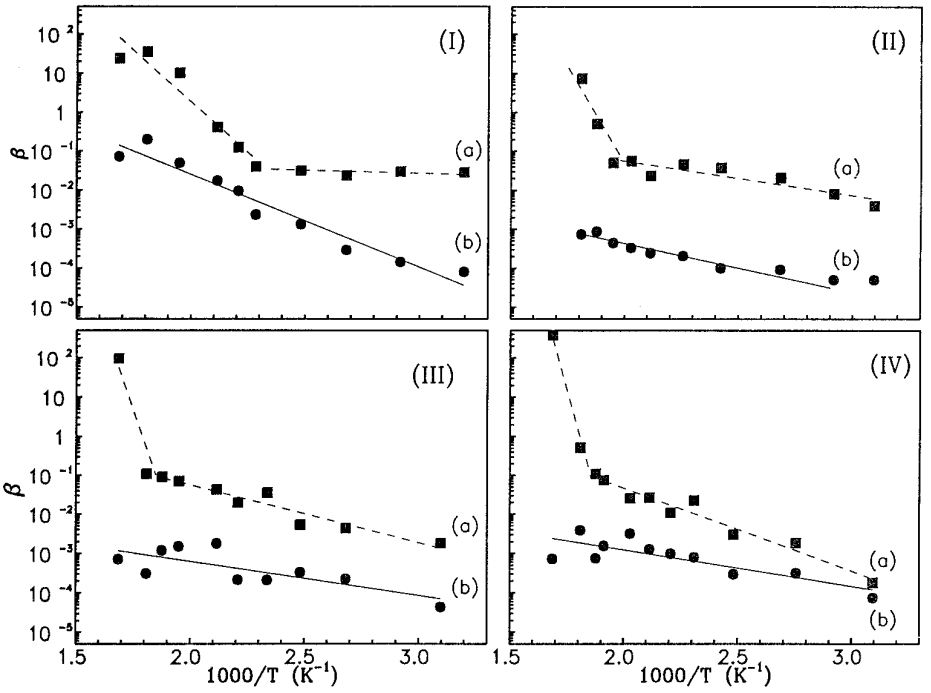

FIG. 8. Arrhenius-type diagrams of the kinetic parameter β of the Elovich equation calculated from the low (a) and high (b) time value linear segments of the curves shown in Fig. 7. Ag–Au composition (wt%): (I) 100–0; (II) 90–10; (III) 70–30; (IV) 50–50.

firmed with carefully designed blank experiments, which were conducted using α-Al_2O_3, that the appearance of this low-temperature TPD feature is not due to gas phase oxygen which had remained in the lines of the apparatus or the reactor but due to an oxygen species originating from the catalyst surfaces, which has previously been assigned to molecularly adsorbed oxygen (13, 27–29). This species appears for all samples and at all adsorption temperatures, even after oxygen adsorption at room temperature. At higher adsorption temperatures (above 100°C) another desorption peak appears with its maximum located between 240 and 300°C, depending on adsorption temperature and sample composition. Upon increasing Au content, this peak shifts to lower desorption temperatures. For example, in the TPD spectra obtained after oxygen adsorption at 200°C the peak maximum shifts from 285°C [Ag–Au (100–0)] to 279 (90–10) to 262 (70–30) to 239°C (50–50). It should be mentioned that for Ag–Au (100–0) this peak is already present at adsorption temperatures of 30°C [Fig. 10(I, a) but absent for the Au-containing samples under the same experimental conditions. At adsorption temperatures above 300°C a third oxygen species, which has previously been identified as subsurface oxygen (13), is clearly observed to desorb. Increasing adsorption temperature causes an increase in the area of the corresponding high-temperature TPD peak, indicating an increase of the population of subsurface oxygen and a shift of its maximum to higher temperatures. Increasing the Au content of the samples leads to smaller TPD peaks and to shifts of the peak maxima to lower desorption temperatures, until the disappearance of the high-temperature peak in the Ag–Au (50–50) TPD spectrum [Fig. 10(IV)].

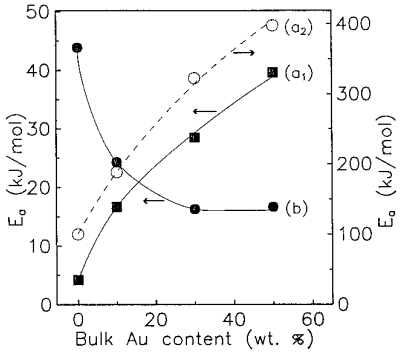

FIG. 9. The activation energy of the three oxygen adsorption processes on the 15% (Ag–Au)/α-Al_2O_3 catalysts as a function of the Au content. (a_1) Atomic oxygen; (a_2) subsurface oxygen; (b) molecular oxygen.

The total amount of desorbed oxygen and that of oxygen desorbed above 200°C, calculated from the TPD spectra of all samples, as a function of adsorption temperature are presented in Table 2. A maximum in the amount of adsorbed oxygen at 200°C and a new increase at adsorption

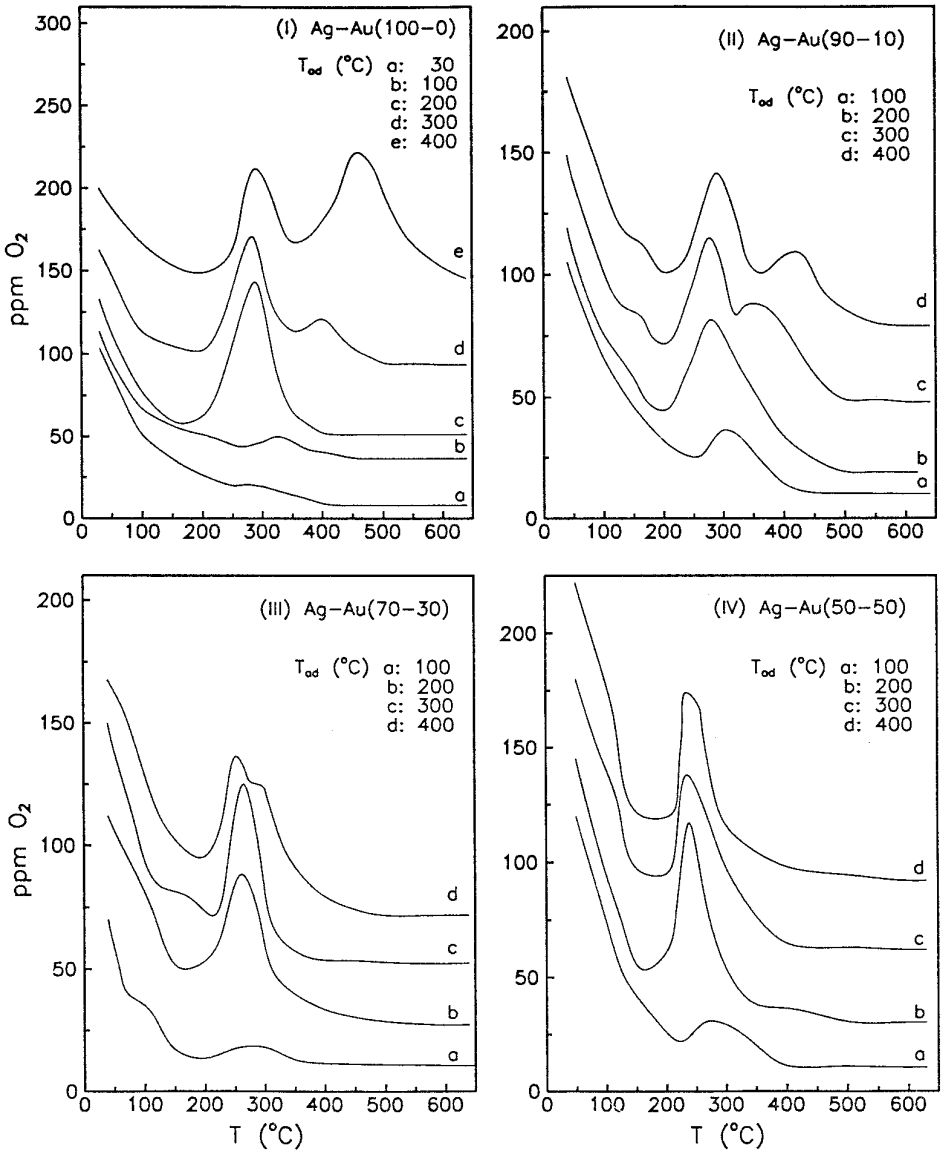

FIG. 10. TPD profiles "spectra" obtained following oxygen adsorption on the 15% (Ag–Au)/α-Al_2O_3 catalysts for 30 min, in the temperature range of 30 to 400°C. β = 20°C/min; Ag–Au composition (wt%): (I) (100–0); (II) (90–10); (III) (70–30); (IV) (50–50).

temperatures above 300°C, especially for catalysts rich in Ag, are observed. These results are qualitatively similar to those obtained using the gravimetric technique (Fig. 5). There is, however, a difference by a factor of 2 in the amount adsorbed, as estimated from the TPD (Table 2) and microgravimetric (Fig. 5) experiments. This difference could be explained by taking into account the different procedures applied in the two experiments. First, in the gravimetric experiments oxygen adsorption took place for 15 h, compared to 30 min in the TPD experiments. Oxygen adsorption continued slowly for many hours [Fig. 6(I–IV)], making it reasonable to expect differences in the amount of adsorbed oxygen upon changing time of adsorption by a factor of 30. Since subsurface oxygen diffusion is a time-dependent process, it is expected that exposing the same surface under the same dose of oxygen will not result in the same relative population of adsorbed oxygen species if the time and pressure of exposure are different. Subsurface diffusion is expected to be favored at longer exposure times. Second, before the TPD experiments were begun, the reactor was flushed with He for 5 min, a step that could remove a certain amount of weakly chemisorbed oxygen.

In another set of TPD experiments the effect of changing the heating rate, β, on the atomic oxygen desorption peak was studied. This kind of experiment can give information concerning the bond strength of the adsorbed gas with the

TABLE 2

The Amount of Oxygen Desorbed from the 15% (Ag–Au)/α-Al_2O_3 Catalysts after Oxygen Adsorption in the Temperature Range of 30 to 400°C

wt% Ag–Au composition	Adsorption temperature (°C)	Total amount of desorbed O_2 (μg/g cat.)	O_2 desorbed above 200°C (μg/g cat.)
100–0	30	36.0	13.8
	100	36.6	17.6
	200	55.8	38.7
	300	52.0	37.0
	400	73.4	60.0
90–10	100	28.1	10.0
	200	39.6	20.3
	300	41.5	24.7
	400	44.5	25.1
70–30	100	21.0	7.2
	200	28.3	16.3
	300	31.5	15.8
	400	35.8	18.8
50–50	100	20.8	7.3
	200	29.1	14.4
	300	25.7	12.9
	400	28.2	13.5

surface through the desorption temperature at the maximum of the TPD peak, T_M, by plotting $\ln[T_M)^2/\beta]$ as a function of $1/T_M$ (30). When TPD experiments take place under UHV conditions the slope of the resulting straight lines gives the activation energy of desorption, E_d, while when desorption occurs under the flow of an inert gas (much slower rate of removal of the desorbed gas) the values obtained correspond to the heat of adsorption, ΔH_a (31, 32).

TPD spectra using different heating rates (20–100°C) were obtained from the Ag–Au/α-Al_2O_3 catalysts after oxygen adsorption at 200°C for 30 min. A typical set of these spectra obtained from Ag–Au (50–50) is shown in Fig. 11. It is observed that the peak maximum shifts to higher desorption temperatures with increasing β. This shift was found to be more pronounced for catalysts rich in gold. It is also observed that the desorption peak of the weakly chemisorbed species that desorbs below 150°C is more clearly resolved (Fig. 11). As stated above, knowledge of the peak maximum shift, T_M, of a TPD spectral feature as a function of the heating rate, β, enables the calculation of the heat of adsorption, ΔH_a, of the adsorbed species (31, 32) to be made. The data obtained from the corresponding TPD spectra plotted in these coordinates are shown in Fig. 12(I). From the slopes of the straight lines which are formed, the values of ΔH_a for atomic oxygen adsorption on the Ag–Au surfaces were obtained. The resulting values of ΔH_a are presented in Fig. 12(II). It is obvious that increasing the catalyst surface composition in Au results in a decrease in ΔH_a, which reflects weakening of the Ag–O bond.

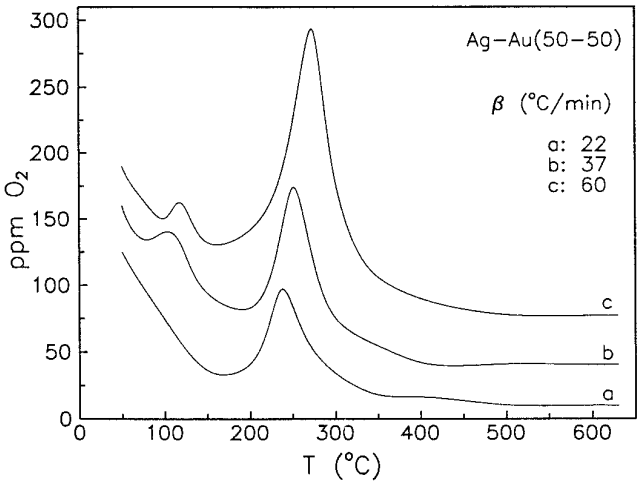

FIG. 11. The effect of heating rate, β, on the TPD spectra obtained from the Ag–Au (50–50) catalyst after oxygen adsorption at 200°C for 30 min.

DISCUSSION

(*i*) *Oxygen Adsorption Kinetics*

The results of the gravimetric experiments (Figs. 5–9) reveal the existence of three kinetically distinguishable adsorption processes on the Ag–Au/α-Al_2O_3 catalysts, in agreement with results obtained using monometallic Ag/α-Al_2O_3 (12–14). Two of the adsorption processes are present over the entire temperature range examined (40–320°C). One is dominant at low surface coverages and has previously been attributed to dissociative oxygen adsorption, a process that was found to require multiple surface sites to occur (13). The second adsorption process takes place in parallel with the former and is due to molecular oxygen adsorption, as was found on monometallic Ag/α-Al_2O_3 catalysts using SERS (12), microgravimetric, and temperature desorption (13) techniques. Molecular oxygen adsorption is dominant at surface coverages above 0.2–0.5, depending on the adsorption temperature and alloy composition (Fig. 7). Finally, a third process, which has previously been attributed to diffusion of oxygen to subsurface sites, based on results obtained using isotopically labeled oxygen (13), is initiated at temperatures above 165°C, depending on alloy composition (Fig. 8).

Alloying silver with gold induces significant changes in the mode of oxygen adsorption on Ag, as observed in the microgravimetric experiments (Figs. 5–9). These changes depend on the Au content of the catalysts. It is interesting

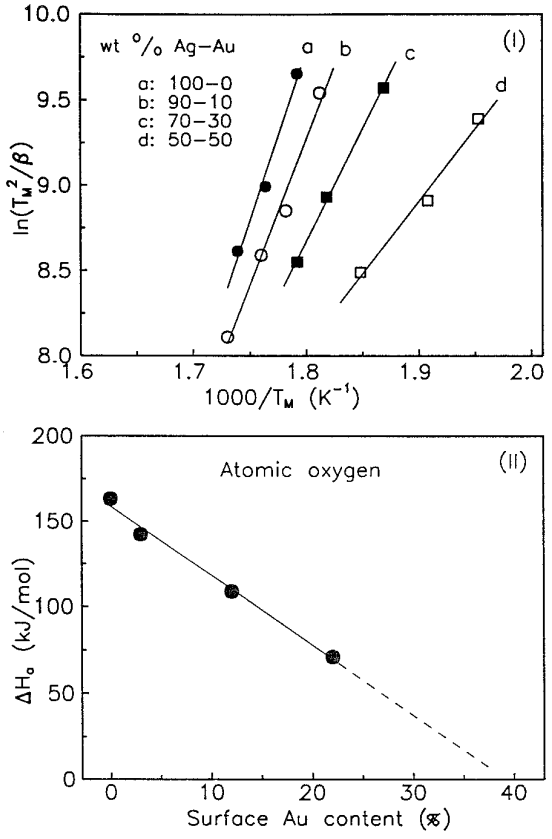

FIG. 12. (I) Plot of $\ln(T_M^2/\beta)$ as a function of $1000/T_M$ (Eq. [4]) for calculating the heat of adsorption of atomic oxygen on the 15% Ag–Au)/α-Al_2O_3 catalysts. (II) The dependence of the heat of adsorption of atomic oxygen on the surface Au content of the 15% (Ag–Au)/α-Al_2O_3 catalysts.

to note that the significant decrease of the total amount of oxygen adsorbed at equilibrium on the Ag–Au (90–10) sample relative to Ag–Au (100–0), especially at adsorption temperatures above 160–180°C (Fig. 5, curves a and b). This behavior implies that a relatively small quantity of Au on the catalyst surface is enough to inhibit to a significant extent an adsorption process, probably dissociative adsorption, which requires multiple sites of adjacent Ag atoms to proceed (13). In accordance with previous studies (6–8) it is suggested that Au atoms act as a "diluting agent" on the Ag surface, destroying the multiple adsorption sites mentioned above, thus hindering atomic oxygen adsorption even when Au is present in small quantities. According to this hypothesis, further increase of the Au content is not expected to induce similarly drastic changes in the atomic oxygen adsorption process, because the degree of destruction of the corresponding sites is not proportional to the Au composition of the alloy crystallites. This seems to be the case in our experiments since, as shown in Fig. 5, increasing Au content above 10 wt% leads to a less drastic decrease of the amount of adsorbed oxygen. These results are in accordance with the early work of Kilty *et al.* (33), who studied the effect of chlorine on the chemisorptive properties of Ag. The authors reported that a chlorine coverage of 0.25 is enough to selectively block the sites on which oxygen adsorbs dissociatively and to completely eliminate product formation during the ethylene oxidation reaction (33). Furthermore, Toreis and Verykios (6) have calculated, using a Monte Carlo simulation, that the number of available four-adjacent Ag atom sites becomes very small or zero for surfaces which contain more than 30 at.% Au. Results of the present study confirm the above findings. The maxima observed at approximately 200°C in the equilibrium oxygen adsorption curves (Fig. 5) are mainly due to atomically adsorbed oxygen. It is observed that the heights of the maxima decrease with increasing Au content [Fig. 5(a–e)] and almost disappear for the Ag–Au (50–50) sample (curve d), indicating destruction of multiple sites for dissociative oxygen adsorption.

The increasing difficulty of atomic oxygen adsorption with increasing Au content is also reflected in the observed changes in the activation energy of atomic oxygen adsorption upon varying alloy composition (Fig. 9). The activation energy (at zero surface coverage) for dissociative adsorption monotonically increases from 4 to 40 kJ/mol with increasing Au content from 0 to 24 surface at.% [Fig. 9 (curve a_1)]. The increase of E_a probably reflects the increasing difficulty for atomic oxygen adsorption to occur due to geometric-type restrictions that exist from the destruction of the multiple Ag atom sites by Au atoms.

A second adsorption process occurs in parallel with dissociative adsorption over the whole temperature range examined and is due to molecular oxygen adsorption (12–14). Although there is still a debate concerning the existence of a dioxygen species in the adsorbed mode at elevated temperatures, several recent studies reveal that such a species exists on Ag surfaces [27] and especially on Ag modified by alkalis (28, 29, 34, 35) or chlorine (36–38). Recently, Wu *et al.* (38) studied the effect of chlorine on oxygen adsorption on Ag(111) using HREELS and TPD. Even in the absence of chlorine the authors observed a molecular oxygen species adsorbed on special defect sites at room temperature. When the single crystal was exposed to a relatively high chlorine dose the rate of oxygen adsorption on Ag(111) increased, the molecular oxygen species, argued by the authors to be adsorbed on special defect sites, became more stable at room temperature, and subsurface diffusion of atomic oxygen was promoted (38). In our previous study (12) we have observed, using SERS, the existence of an intense band at 815 cm^{-1} after exposing polycrystalline Ag samples to oxygen, and assigned it to the ν(O–O) stretching vibration of a molecularly adsorbed oxygen species, with its axis lying perpendicular to the Ag surface. This species was found to be present at high temperatures and under ethylene epoxidation reaction conditions (12).

Since molecular oxygen adsorption probably does not require multiatom adsorption sites (12, 13), it is expected to be favored by the presence of Au. It is argued that upon interaction of oxygen with a clean Ag surface, the initial, kinetically important, adsorption step is dissociative chemisorption, with the oxygen adatoms occupying multicoordinated sites. The precursor of this process is probably molecularly adsorbed oxygen, lying with its axis parallel to the surface. After this process has taken place to a certain extent and not many multiple sites are available, there still exist uncovered single Ag atom sites on which atomic oxygen adsorption is not possible. It is on these, sporadically free, single Ag atom sites that molecular oxygen may adsorb with its axis perpendicular to the surface. Alloying silver with gold induces the creation of these single Ag atom sites, since Au acts as a diluting agent on the Ag surface. The result of alloying is then to favor molecular versus atomic oxygen adsorption.

The dependence of activation energy for molecular oxygen adsorption on Ag–Au composition shows a trend opposite to that of atomic oxygen (Fig. 9), confirming that the two species adsorb on different surface sites. It may be suggested that the relatively high activation energy of molecular oxygen adsorption at zero coverage on the Ag–Au (100–0) sample (44 kJ/mol) contains a term that reflects the difficulty of finding free adsorption sites upon initiation of the adsorption process. The kinetically much faster atomic oxygen adspecies rapidly cover the surface, thus inhibiting molecular oxygen adsorption, which takes place on isolated Ag atoms only after the energetically favored dissociative adsorption has proceeded to a significant extent. Alloying Ag with gold favors molecular oxygen adsorption due to the creation of new single Ag sites which cannot be occupied by atomic oxygen and leads to a decrease of the apparent activation energy of the adsorption process.

The third oxygen adsorption process, which is initiated at relatively high adsorption temperatures and has previously been attributed to subsurface oxygen diffusion (13), is also significantly affected by the presence of Au. As observed in Fig. 5, the increase of the equilibrium oxygen uptake observed for the Ag–Au (100–0) and Ag–Au (90–10) samples at temperatures above 220–230°C is not observed on the Ag–Au (70–30) and (50–50) samples, where only slight maxima are observed at approximately 250°C. This behavior indicates that oxygen diffusion to subsurface sites is hindered with increasing Au content. This is more clearly shown in the Arrhenius-type diagrams of Fig. 8(I–IV). The presence of subsurface oxygen becomes pronounced at temperatures above 165°C on the Ag–Au (100–0) sample as indicated by the breaking point of curve (a) in Fig. 8(I) which marks the temperature of initiation of the process over this catalyst. Upon alloying Ag with Au, the breaking point gradually shifts to higher adsorption temperatures, and for the Ag–Au (50–50) catalyst it appears at ~270°C [(Fig. 8(I–IV)], indicating that the presence of Au hinders subsurface diffusion of atomic oxygen which is now initiated at significantly higher temperatures.

This hindrance of subsurface diffusion is also reflected in the increase of the activation energy of the process with increasing Au content (Fig. 9). The activation energy of subsurface diffusion on monometallic Ag/α-Al_2O_3 is 100 kJ/mol, in very good agreement with the value of 96 kJ/mol calculated by Ramanarayanan and Rapp (39) for the activation energy of dissolution of oxygen in bulk Ag in electrochemical experiments conducted in the temperature range of 750 to 950°C. Upon alloying Ag with Au, the activation energy of the process increases significantly from 100 kJ/mol in the Ag–Au (100–0) to 400 kJ/mol for the Ag–Au (50–50) sample. The cause of this behavior is further discussed in the following paragraphs, along with the TPD results.

(*ii*) *Oxygen Desorption Studies*

The results of the TPD experiments are in harmony with those obtained with the gravimetric method. In the oxygen desorption spectra obtained from the 15% (Ag–Au)/α-Al_2O_3 catalyst surfaces (Figs. 10 and 11) three TPD features are observed, depending on adsorption temperature and surface composition of the sample. As was discussed in a previous publication (13), the weakly adsorbed species that desorbs at temperatures below 150°C is due to molecular oxygen, the peak at 285°C is due to atomic oxygen, and the high-temperature peak which emerges only after oxygen adsorption at temperatures above 300°C is due to subsurface oxygen.

Alloying Ag with Au affects the TPD spectral features in several ways. The peak maximum of atomic oxygen shifts monotonically toward lower desorption temperatures with increasing Au content, as shown in Fig. 10(I–IV). This result indicates that the presence of Au atoms on the surface causes weakening of the Ag–O bond, a property which is also reflected in the decrease of the heat of adsorption of this species with increasing Au content of the surface [(Fig. 12(II)]. Similar observations were made by Toreis and Verykios (6), who explained their results evoking electronic-type alterations induced to the Ag atoms by the presence of neighboring Au atoms. XPS experiments have shown (40) that in the Ag–Au alloys there is a transfer of conductive *s*- and *p*-electrons from Ag to Au atoms and a compensating charge transfer in the opposite direction. The net result is that upon alloying Ag with Au the Ag atoms ''lose'' electrons, which is also in accordance with the relative value of the work function of the two metals. Since the work function of Ag (4.64 eV) is lower than that of Au (5.32 eV) (41), electronic interactions between the two metals are expected to lead to charge transfer from

Ag to Au. Considering the fact that dissociative adsorption of oxygen on Ag requires charge transfer from Ag to oxygen, it is expected that the electron deficiency induced on Ag atoms by the presence of neighboring Au atoms or the increase of the surface work function will result in weakening of the Ag–O bonds. The fact that the dissociative adsorption of oxygen on Ag is directly related to the surface work function has been demonstrated by Dean and Bowker (28), who employed preadsorbed alkali promoters to alter the work function of the surface. The TPD experiments of Fig. 10(I–IV), which also show that weakening of the Ag–O bond is proportional to the surface Au composition, can thus be explained by evoking an electronic interaction between the dissimilar neighboring atoms in the alloy crystallites, which results in enhancement of the surface work function.

A measure of the Ag–O bond strength is given by the heat of adsorption, ΔH_a. As shown in Fig. 12(II), ΔH_a decreases linearly with increasing surface Au content. It is interesting to note that if this linearity holds for Au contents higher than those examined, the heat of atomic oxygen adsorption will become zero for catalysts containing more than 35–40% surface Au atoms, which would induce drastic changes in the catalytic phenomena over these surfaces. Indeed, as was shown in kinetic experiments performed with this series of Ag–Au alloy catalysts, catalytic activity ceases over surfaces which contain more than 40 at.% Au (14, 42).

The population of molecularly adsorbed oxygen increases in quantity with increasing Au content. This is expected since, as was discussed in previous paragraphs, surface Au atoms act as a ''diluting agent,'' destroying multiple Ag atom sites required for atomic oxygen adsorption and thus creating new adsorption sites for molecular oxygen adsorption. The electronic deficiency of Ag atoms induced by alloying is expected to inhibit molecular oxygen adsorption as in the case of atomic oxygen. The magnitude of this effect is expected to be less pronounced in the case of molecular oxygen because it is less polar than atomic oxygen and, as a result, the electronic-type effect is not expected to be equally important for this adsorption process. The net result is that molecular oxygen adsorption is enhanced since the favoring effect of the geometric factor overcomes any inhibiting effect of the electronic factor.

Alloying Ag with Au also induces significant alterations in the high-temperature TPD feature which has been assigned to subsurface oxygen (Fig. 10). It should be mentioned here that the term ''subsurface'' is used in its most general meaning, to describe the species that diffuse below the surface. It is possible that the observed subsurface species is due to bulk oxide, which has been found to desorb at temperatures similar to those of atomic oxygen (29, 43). For the Ag–Au (90–10) sample [Fig. 10(II)], there is a shift of the peak maximum toward lower desorption temperatures and a decrease of its height, compared to the Ag–Au (100–0) sample [Fig. 10(I)]. A further increase in the Au content to Ag–Au (70–30) results in a significant decrease in the high-temperature peak intensity which is only visible as a shoulder to the atomic oxygen peak in the TPD spectrum following adsorption at 400°C [Fig. 10(III)]. Finally, the high-temperature peak is absent in the Ag–Au (50–50) sample, indicating that in this case subsurface diffusion is strongly inhibited [Fig. 10(IV)].

These results indicate either that subsurface diffusion does not take place on catalysts rich in Au, in the temperature range examined, or that oxygen diffuses only to the first subsurface layer of Ag in the Au-rich sample and, thus, desorbs at temperatures very close to those of atomic oxygen, making the corresponding TPD peaks indistinguishable under the experimental conditions used. It was demonstrated, using the gravimetric technique, that subsurface diffusion is highly activated, and, as a result, this process becomes significant only at high temperatures (Fig. 8). For the Ag–Au (100–0) sample the process is initiated at temperatures above 165–180°C [(Fig. 9 (curve a_2)]. As can be observed in Fig. 8(I–IV), increasing Au content leads to an increase of the activation energy of the process, which results in a shift of the temperature of initiation of the process toward higher values [Fig. 8(I–IV)]. The TPD spectra shown in Fig. 10(I–IV) are in accordance with these results. An increasing Au content of the surface results in a decrease of the area of the high-temperature TPD peak, for a fixed adsorption temperature, and a shift of the maximum of the peak toward lower desorption temperatures, until it is not observed in the TPD spectra obtained from the Ag–Au (50–50) sample [Fig. 10(IV)].

The driving force for subsurface diffusion is related to the fact that atomic oxygen adsorbed on the Ag surface is unstable compared with the subsurface species, for which the coordination number with the Ag atoms has the maximum possible value. Oxygen incorporation into the subsurface region has been observed for many metal–oxygen systems even at temperatures as low as 77 K, as reported for Zn and Fe (44). For the fcc metals it has been found that the extent of oxygen diffusion to subsurface sites is proportional to the interatomic distance of the metal atoms in the (100) direction (44). Ertl and co-workers (45, 46) argue that O atoms fit perfectly in the octahedral holes of the Ag lattice. The same authors detected two kinds of dissolved oxygen species in Ag films in their TDS experiments and assigned them to oxygen dissolved in the subsurface region and to oxygen dissolved in the Ag bulk. Similar were the findings of Bowker *et al.* (47).

The driving force that attracts the chemisorbed ''ion'' toward the subsurface region can be related to the ''image force'' (44)

$$F = q^2/4 \cdot k \cdot x^2, \qquad [3]$$

where q is the charge of the adsorbed species, k is the dielectric constant, and x is the distance of the chemisorbed species from the metallic surface. According to this model [44], the activation energy, E, for subsurface diffusion is given by

$$E = W - a \cdot (q^2/4 \cdot k \cdot x^2), \qquad [4]$$

where W is the activation energy in the absence of the image force, and a is the distance moved by the cation. The value of W can be approximated by the metal–metal bond strength (44). In the case in which E is positive, subsurface diffusion will be an activated process. The bond strengths of Ag–Ag, Ag–Au, and Au–Au are approximately 165, 200, and 225 kJ/mol, respectively (48). It is therefore to be expected that upon increasing the Au content of the Ag–Au catalysts, the average bond strength between the atoms of the alloy will also be increased with a resultant increase of W and a concomitant increase of the activation energy for subsurface diffusion (Eq. [4]). This simple model can give only qualitative information because it does not take into account parameters that may also affect the process, such as restrictions of geometric type.

Another possible reason for the observed hindrance of subsurface diffusion caused by the presence of Au atoms could be related to alterations in the interatomic distances which occur upon alloying Ag with Au. As discussed in a previous paragraph, the lattice parameter, a_0, decreases linearly with increasing Au content, in the composition range of interest (Fig. 2). Although the decrease in the interatomic distances is small, it could offer an additional, geometric type, restriction in the subsurface diffusion process.

The population of subsurface oxygen is also thermodynamically limited. Since subsurface oxygen is in equilibrium with surface atomic oxygen, it is expected that the decrease of the atomic oxygen population induced by the presence of Au will result in a decrease of the population of subsurface oxygen, too. This is expected to result in diffusion of atomic oxygen to fewer subsurface Ag layers and, as a result, to a shift of the desorption temperature of the TPD peak towards lower temperatures.

Although all of these factors contribute in the observed alterations of subsurface oxygen diffusion, upon alloying Ag with Au, in all probability electronic-type interactions play the most significant role, as in the case of atomic oxygen. The charge transfer from Ag to Au which takes place upon alloying results in decrease of the strength of the ''driving force'' which governs the subsurface diffusion process and attracts the atomically adsorbed oxygen to diffuse into the alloy lattice.

CONCLUSIONS

The existence of three oxygen species in the adsorbed mode on α-Al_2O_3-supported Ag–Au alloy crystallites was probed using microgravimetric and TPD techniques. The presence of Au on the Ag surfaces leads to destruction of multiple sites necessary for dissociative oxygen adsorption. Upon increasing Au content from zero to 24 surface at.% the activation energy (at zero surface coverage) of adsorption of atomic oxygen gradually increases form 4 to 40 kJ/mol. The Ag–O bond weakens due to electronic-type interactions between Ag and neighboring Au atoms, and the enthalpy of adsorption decreases linearly with surface Au content, to essentially zero at surfaces containing more than 40 at.% Au. On the other hand, the activation energy for molecular oxygen adsorption decreases from 44 to 17 kJ/mol upon increasing Au content from zero to 24%. The opposite influence of the presence of Au on the activation energies of adsorption of atomic and molecular oxygen indicates that these species adsorb on different surface Ag sites. Subsurface oxygen diffusion is strongly hindered by the presence of Au and the activation energy of this process increases from 100 kJ/mol for pure Ag to 400 kJ/mol for surfaces containing 24% Au. In the latter case, subsurface oxygen diffusion does not take place even at adsorption temperatures of 400°C.

REFERENCES

1. Verykios, X. E., Stein, F. P., and Couglin, R. W., *Catal. Rev. Sci. Eng.* **22,** 197 (1980).
2. Sachtler, W. M. H., Backx, C., and van Santen, R. A., *Catal. Rev. Sci. Eng.* **23,** 127 (1981).
3. Barteau, M. A., and Madix, R. J., *in* ''The Chemical Physics of Solid Surfaces and Heterogeneous Catalysis'' (D. A. King and P. Woodruff, Eds.), Vol. 4, p. 95. Elsevier, Amsterdam, 1982.
4. van Santen, R. A., and Kuipers, H. P. C. E., *in* ''Advances in Catalysis'' (D. D. Eley, H. Pines, and P. B. Weisz, Eds.), Vol. 35, p. 265, Academic Press, New York, 1987.
5. Srivastava, R. D., *in* ''Heterogeneous Catalytic Science,'' CRC Press, Boca Raton, FL, 1988.
6. Toreis, N., and Verykios, X. E., *J. Catal.* **108,** 161 (1987).
7. Herrera, R. N., Martinez, E. N., and Varma, A., Presented at AIChE Ann. Meeting, Chicago, IL, 1985.
8. Herrera, R., Varma, A., and Martinez, E., ''Proc. Int. Symp. New Developments in Selective Oxidation,'' Rimini, Italy, 1989.
9. Mehrotra, P., and Verykios, X. E., *J. Catal.* **88,** 409 (1984).
10. Bonin, R. and Verykios, X. E., *J. Catal.* **91,** 36 (1985).
11. Toreis, N., Verykios, X. E., Chalid, S. M., Bunker, G., and Korszum, Z. R., *J. Catal.* **109,** 143 (1988).
12. Kondarides, D. I., Papatheodorou, G. N., Vayenas, C. G., and Verykios, X. E., *Ber. Bunsenges. Phys. Chem.* **97,** 709 (1993).
13. Kondarides, D. I., and Verykios, X. E., *J. Catal.* **143,** 481 (1993).
14. Kondarides, D. I., and Verykios, X. E., *Stud. Surf. Sci. Catal.* **82,** 471 (1994).
15. Briggs, D., and Seah, M. P., *in* ''Practical Surface Analysis,'' 2nd ed., Wiley, 1990, New York.
16. Cullity, B. D., ''Elements of X-Ray Diffraction,'' Addison–Wesley, Reading, MA, 1959.

17. Pearson, W. B., ''Handbook of Lattice Spacings and Structure of Metals,'' Pergamon, London, 1967.
18. Somorjai, G. A., ''Chemistry in Two Dimensions: Surfaces,'' Cornell Univ. Press, Ithaca, NY, 1981.
19. Delannay, F., ''Characterization of Heterogeneous Catalysts,'' Decker, New York, 1984.
20. Campbell, C. T., *Annu. Rev. Phys. Chem.* **41,** 775 (1990).
21. Gavriilidis, A., Sinno, B., and Varma, A., *J. Catal.* **139,** 41 (1993).
22. Scholten, J. J. F., Konvalinka, J. A., and Beckman, F. W., *J. Catal.* **28,** 209 (1973).
23. Seydmonir, S. R., Strohmayer, D. E., Geoffroy, G. L., Vannice, M. A., Young, H. W., and Linowski, J. W., *J. Catal.* **87,** 424 (1984).
24. Matyi, R. J., Schwartz, L. H., and Butt, J. B., *Catal. Rev. Sci. Eng.* **29,** 41 (1987).
25. Aharoni, C., and Tompkins, F. C., *Adv. Catal.* **21,** 1 (1970).
26. Rehren, C., Muhler, M., Bao, X., Schlögl, R., and Ertl, G., *Z. Phys. Chem.* **174,** 11 (1991).
27. Grant, R. B., and Lambert, R. M., *Surf. Sci.* **146,** 256 (1984).
28. Dean, M., and Bowker, M., *J. Catal.* **115,** 138 (1989).
29. Dean, M., McKee, A., and Bowker, M., *Surf. Sci.* **211/212,** 1067 (1989).
30. Boudart, M., and Djéga-Mariadassou, ''Kinetics of Heterogeneous Catalytic Reactions,'' Princeton Univ. Press, Princeton, NJ, 1984.
31. Konvalinka, J. A., Scholten, J. J. F., and Rasser, J. C., *J. Catal.* **48,** 365 (1977).
32. Herz, R. J., Kiela, J. B., and Martin, S. P., *J. Catal.* **73,** 66 (1982).
33. Kilty, P. A., Rol, N. C., and Sachtler, W. M. H., Proc. 5th Int. Cong. Catal., Palm Beach, 1972, (J. W. Hightower, Ed.), p. 929, North Holland, Amsterdam, 1973.
34. Spencer, N. P., and Lambert, R. M., *Surf. Sci.* **104,** 63 (1981).
35. Spencer, N. P., and Lambert, R. M., *Chem. Phys. Lett.* **83,** 388 (1981).
36. Kamath, P. V., Prabhakaran, K., and Rao, C. N. R., *Surf. Sci.* **146,** L551 (1984).
37. Tan, S. A., Grant, R. B., and Lambert, R. M., *J. Catal.* **100,** 383 (1986).
38. Wu, K., Wang, D., Wei, X., Cao, Y., and Guo, X., *J. Catal.* **140,** 370 (1993).
39. Ramanarayanan, T. A., and Rapp, R. A., *Metal. Trans.* **3,** 3239 (1972).
40. Watson, R. E., Hudis, J., and Perlman, M. L., *Phys. Rev. B* **4,** 4139 (1971).
41. ''Lange's Handbook of Chemistry'' (J. A. Dean, Ed.), 4th ed., McGraw–Hill, New York, 1992.
42. Kondarides, D. I., and Verykios, X. E., manuscript in preparation.
43. Bowker, M., *Surf. Sci.* **155,** L276 (1985).
44. Roberts, M. W., and McKee, C. S., ''Chemistry of the Metal Gas Interface,'' Oxford Univ. Press, Oxford, 1978.
45. Rehren, C., Isaac, G., Schlögl, R., and Ertl, G., *Catal. Lett.* **11,** 253 (1991).
46. Bao, X., Bath, J. V., Lehmpfuhl, G., Schuster, R., Uchida, Y., Schlögl, R., and Ertl, G., *Surf. Sci.* **284,** 14 (1993).
47. Bowker, M., Pudney, P., and Roberts, G., *J. Chem. Soc. Faraday Trans. I* **85,** 85 (1989).
48. ''Handbook of Chemistry and Physics,'' 66th ed. CRC Press, Boca Raton, FL, 1985.